ANESTHESIOLOGY

Positional Therapy and Regional Pulmonary Ventilation

High-resolution Alignment of Prone and Supine Computed Tomography Images in a Large Animal Model

Yi Xin, M.S., Maurizio Cereda, M.D., Hooman Hamedani, M.S., Kevin T. Martin, B.S., Nicholas J. Tustison, Ph.D., Mehrdad Pourfathi, Ph.D., Stephen Kadlecek, Ph.D., Sarmad Siddiqui, Ph.D., Faraz Amzajerdian, B.S., Marc Connell, M.S., Nicholas Abate, B.A., Agi Kajanaku, B.A., Ian Duncan, Ph.D., James C. Gee, Ph.D., Rahim R. Rizi, Ph.D.

Anesthesiology 2020; 133:1093–105

EDITOR'S PERSPECTIVE

What We Already Know about This Topic

- Prone positioning in severe adult respiratory distress syndrome has been shown to improve oxygenation and reduce mortality.
- Previous imaging studies have been limited to evaluation of gravitational effects and have not considered tissue deformation or its effects on regional gas content or on small units of tissue.
- Other authors have previously reported craniocaudal changes in ventilation and perfusion in the vicinity of the diaphragm in the prone position not explained by gravity.

What This Article Tells Us That Is New

- The authors utilized their previously reported computed tomography data from five mechanically ventilated sedated pigs before and after lung injury by tracheal administration of hydrocholoric acid to assess positional inflation characteristics in response to supine and prone positioning and two levels of positive end-expiratory pressure (5 and 10 cm H_2O) applied in random order.
- Regional cluster distributions of units of paired, digitally aligned prone and supine lung tissue according to density and deformation dimensions (deflation, stable density/volume, and reinflation) were analyzed.
- Patterns followed both gravitational and nongravitational distributions. Reinflation was concentrated in the caudal lung region near the dorsal portion of the diaphragm.
- Recruitment of nonaerated tissue contributed to reinflation in this region after injury.
- The demonstrated clinical benefits of prone positioning may be related to localized changes (recruitment or reinflation) in the dorso–caudal lung region, a hypothesis that awaits further testing.

ABSTRACT

Background: Prone ventilation redistributes lung inflation along the gravitational axis; however, localized, nongravitational effects of body position are less well characterized. The authors hypothesize that positional inflation improvements follow both gravitational and nongravitational distributions. This study is a nonoverlapping reanalysis of previously published large animal data.

Methods: Five intubated, mechanically ventilated pigs were imaged before and after lung injury by tracheal injection of hydrochloric acid (2 ml/kg). Computed tomography scans were performed at 5 and 10 cm H_2O positive end-expiratory pressure (PEEP) in both prone and supine positions. All paired prone–supine images were digitally aligned to each other. Each unit of lung tissue was assigned to three clusters (K-means) according to positional changes of its density and dimensions. The regional cluster distribution was analyzed. Units of tissue displaying lung recruitment were mapped.

Results: We characterized three tissue clusters on computed tomography: deflation (increased tissue density and contraction), limited response (stable density and volume), and reinflation (decreased density and expansion). The respective clusters occupied (mean ± SD including all studied conditions) 29.3 ± 12.9%, 47.6 ± 11.4%, and 23.1 ± 8.3% of total lung mass, with similar distributions before and after lung injury. Reinflation was slightly greater at higher PEEP after injury. Larger proportions of the reinflation cluster were contained in the dorsal *versus* ventral (86.4 ± 8.5% *vs.* 13.6 ± 8.5%, $P < 0.001$) and in the caudal *versus* cranial (63.4 ± 11.2% *vs.* 36.6 ± 11.2%, $P < 0.001$) regions of the lung. After injury, prone positioning recruited 64.5 ± 36.7 g of tissue (11.4 ± 6.7% of total lung mass) at lower PEEP, and 49.9 ± 12.9 g (8.9 ± 2.8% of total mass) at higher PEEP; more than 59.0% of this recruitment was caudal.

Conclusions: During mechanical ventilation, lung reinflation and recruitment by the prone positioning were primarily localized in the dorso-caudal lung. The local effects of positioning in this lung region may determine its clinical efficacy.

(ANESTHESIOLOGY 2020; 133:1093–105)

VENTILATION in the prone position improves blood gases[1] and decreases mortality in patients with acute respiratory distress syndrome (ARDS).[2] Imaging studies suggest that redistribution of lung inflation along the gravitational axis may explain such beneficial effects. In fact, pulmonary aeration,[3] pleural pressures,[4] and regional strain[5,6] are more homogeneous when subjects are prone rather than supine, due to the apparent attenuation of the gravity-related forces that compress and deform the lungs.[7] Studies evaluated the effects of body position on lung aeration in separate prone and supine computed tomography scans, *e.g.*, by comparing ventro-dorsal gradients of tissue density.[3] However, this approach has limitations. First, it is restricted to measuring the effects of gravity and does not identify positional changes in nongravitational distributions.[8] Second, it is unable to directly measure tissue deformation, or its effect on regional gas content. Third, it cannot measure the effects

<zdoi;. DOI: 10.1097/ALN.0000000000003509>

of position on small units of tissue, as these are not tracked across images. Mapping small-scale changes of lung tissue density and deformation could better characterize patterns of regional inflation associated with the prone position.[9] Fortunately, recent advances in image processing may allow such in-depth assessment of the structural effects of position. For example, cluster analysis allows us to partition large datasets in groups with similar attributes, and can be used for the unrestricted assessment of regional distributions of imaging variables.[10] Image registration provides structural correspondence between paired images[11,12] and allows us to map changes in aeration[13] and lung tissue deformation at high resolution.[14,15] However, this methodology has not yet been used to study positional therapy, since aligning paired prone and supine images is complicated by marked shifts of lung and chest wall geometry between respective positions.

In a previous study, prone positioning contained the progression of experimental lung injury through its beneficial effects on inflation of the dorsal lung.[16] However, previous animal studies comparing prone *versus* supine positions showed craniocaudal changes in ventilation and perfusion in the vicinity of the diaphragm,[8] which were not explained by gravity. These regional gradients are likely explained by nongravitational effects of position on inflation and tissue compression, which have not been directly visualized. In the current study, we reanalyzed our previous pig data[16] to topographically characterize the effects of body position on lung tissue. We hypothesized that improvements in lung aeration and tissue deformation occur in gravitational and nongravitational distributions. For this purpose, we aligned paired prone and supine lung images obtained at two levels of positive end-expiratory pressure (PEEP) before and after lung injury, to produce detailed maps of the effects of prone positioning on each lung tissue unit visible on computed tomography. We then investigated the spatial distribution of position-related changes in density and deformation throughout the lungs using cluster analysis.

Materials and Methods

All studies were approved by the Animal Care and Use Committee of the University of Pennsylvania, Philadelphia, Pennsylvania. Detailed methods are provided in Supplemental Digital Content 1 (http://links.lww.com/ALN/C459). The study is a reanalysis of images included in a previously published article,[16] with uniquely different image analysis methods, nonoverlapping results, and new clinical implications.

Animal Preparation

Five Yorkshire pigs (32.4 ± 2.7 kg) were anesthetized with intramuscular injections of ketamine and xylazine. Pigs were orally intubated, and anesthesia was maintained by continuous intravenous infusion of ketamine and midazolam through a peripheral catheter. Supplemental doses were given to assure immobility during computed tomography scanning. Peripheral oxygen saturation, heart rate, and body temperature were monitored continuously. The femoral artery was catheterized for blood pressure monitoring and arterial blood gas measurement.

Mechanical Ventilation and Lung Injury

Animals were ventilated with a custom-built mechanical ventilator. Tidal volume 8 ml/kg, respiratory rate 15 breaths per minute, and inspired fraction of oxygen 0.6 were constant throughout the experiment. Pigs then received 2 ml/kg hydrochloric acid (pH 1.25) injected in the endotracheal tube over two equally divided doses with the animals alternately in the right and left lateral position. Pigs were then stabilized supine for 60 min with PEEP 10 cm H_2O. Imaging was performed before injury (healthy baseline) as well as after injury and stabilization. Blood gases were obtained after each image acquisition. Airway pressure was monitored using a fiberoptic sensor placed proximally to the endotracheal tube. Tidal volume was recorded from the ventilator display.

Computed Tomography Imaging

Computed tomography scans were acquired with a Siemens (Germany) SOMATOM Force scanner. The settings were as follows: 120 kVp, 200 mAs, pitch 0.95, slice thickness 0.75 mm, collimation 57.6 × 0.6 mm, and estimated dosage 3 to 5 mSv. All images were reconstructed to a resolution of 1 × 1 × 1 mm. End-inspiratory images were obtained during 5-s-long inspiratory pauses, applied during ventilation in both supine and prone positions with PEEP 5 and 10 cm H_2O. Each combination of PEEP and position was applied in random order and maintained for 10 min before imaging, which was shown in pilot studies to assure sufficient stabilization of aeration redistribution. In the prone position, the pigs lay unsupported on their abdomen with their forelegs flexed and their hindlegs extended at the hips. Animals did not receive neuromuscular blocking agents, but sedation was adjusted to achieve immobility, which was confirmed on computed tomography scans by the absence of motion artifacts near the diaphragm.

Image Processing

Our computed tomography analysis (fig. 1) measured changes in computed tomography density (*i.e.*, aeration)

This article is accompanied by an editorial on p. 979. Supplemental Digital Content is available for this article. Direct URL citations appear in the printed text and are available in both the HTML and PDF versions of this article. Links to the digital files are provided in the HTML text of this article on the Journal's Web site (www.anesthesiology.org). Y.X. and M.C. contributed equally to this article.

Submitted for publication February 12, 2020. Accepted for publication July 14, 2020. Published online first on August 4, 2020. From the Department of Radiology (Y.X., H.H., M.P., S.K., S.S., F.A., I.D., J.C.G., R.R.R.) and the Department of Anesthesiology and Critical Care (M.C., K.T.M., M.C., N.A., A.K.), University of Pennsylvania, Philadelphia, Pennsylvania; and the Department of Radiology and Medical Imaging, University of Virginia, Charlottesville, Virginia (N.J.T.).

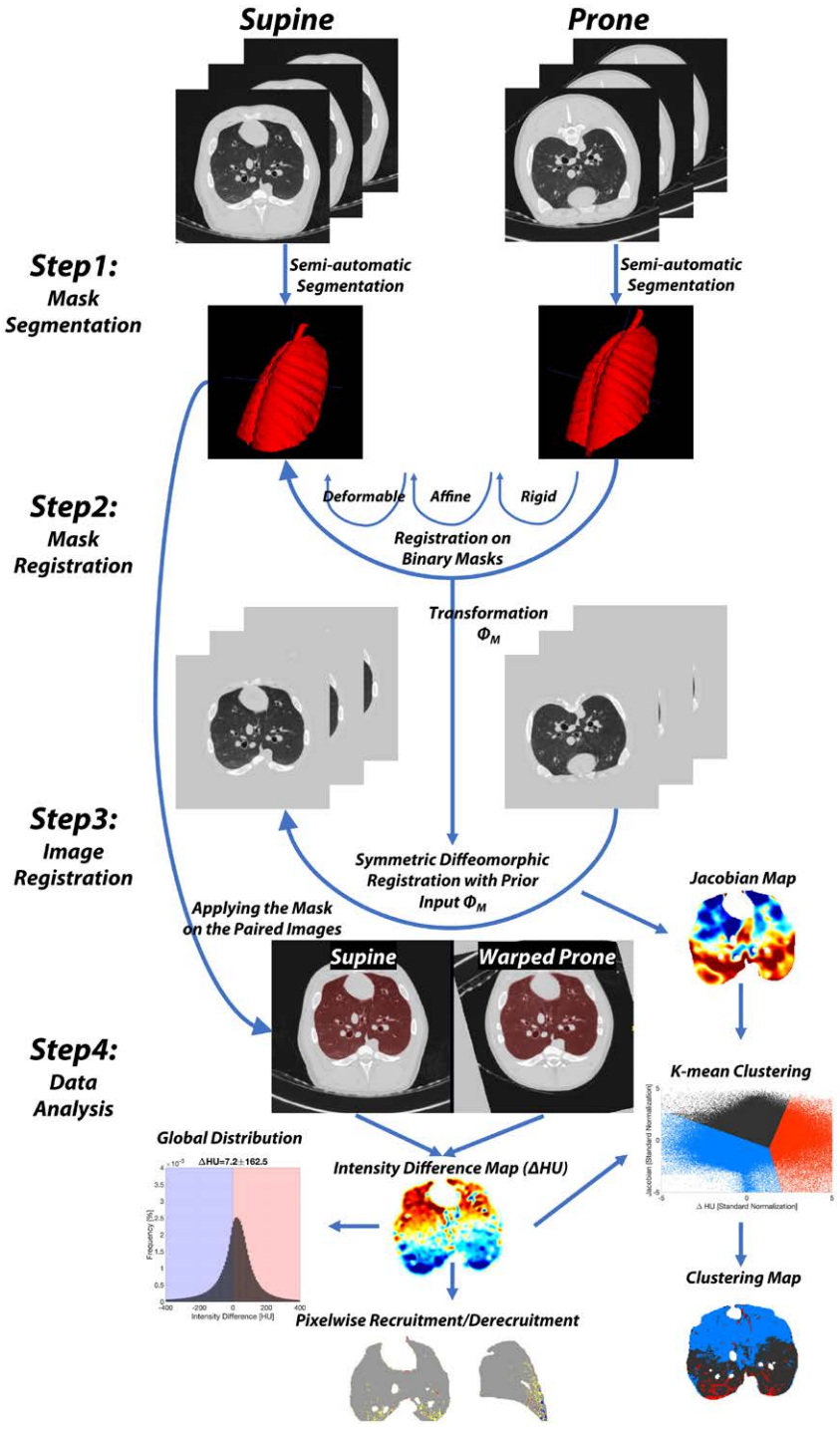

Fig. 1. Outline of image analysis procedures. *Step 1:* A mask outlining the lung borders was obtained for each set of paired supine and prone images. *Step 2:* Each segmented prone mask was registered to the corresponding supine mask using, in sequence: rigid, affine, and deformable registration algorithms, and finally generating a transform (Φ_M). *Step 3:* Registration of the prone to supine image was performed, building on the previously obtained transform Φ_M. A map of the Jacobian was also created during this step to illustrate voxel-by-voxel lung volume changes due to position change. *Step 4:* The masks of the paired images were applied, and further image analysis was performed on the segmented target supine and warped-prone images (shown with inverted orientation to highlight similarities with the target supine image). Finally, subtraction maps and frequency distributions of intensity differences (ΔHU) were created for each pair of supine and prone images. Hounsfield Unit (HU) distributions were used to map lung recruitment and derecruitment with voxel resolution and, together with the Jacobian distributions, to perform cluster analysis of the inflation and deflation characteristics of each voxel.

and dimensions (*i.e.*, spatial deformation) in individual small units (voxels) of tissue. For this purpose, images were registered, *i.e.*, reshaped (warped) and aligned to each other to match the position of each voxel on shared spatial coordinates. This registration corrected for the effects of body position on lung and chest wall geometry. The outlines of the lungs were segmented (separated) from nonpulmonary tissue.

Image Registration and Segmentation. We registered corresponding supine and prone images (fig. 1) using Advanced Normalization Tools.[12,17] The entire registration code is shown as text in Supplemental Digital Content 1 (http://links.lww.com/ALN/C459). During Step 1 of the registration, the outline (mask) of the lungs was segmented from nonpulmonary tissue using previously published methods.[18] In Step 2 of the registration (fig. 1), the prone lung outline was aligned to the supine outline, resulting in a "warped-prone" outline with identical outer geometry to the supine lungs. During Step 3 of the registration, all the pulmonary structures contained within the outlines of the prone and supine computed tomography scans were aligned, yielding a warped image of the prone lungs for each study condition.[11] The quality of the registration was assessed in three ways. First, overlap between the warped-prone and supine lung outlines was quantified using the Dice similarity coefficient. The Dice coefficient was 0.988 ± 0.002 before injury and 0.983 ± 0.006 after injury, suggesting optimal overlap of the lung outlines between warped-prone and supine images. Second, trained operators measured minimal differences in the spatial coordinates of anatomical landmarks between warped-prone and supine images, suggesting conserved spatial orientation of parenchymal structures (see figure, Supplemental Digital Content 2, http://links.lww.com/ALN/C460, showing the results of this analysis). Third, we compared regional density distributions between original and warped prone images (see table, Supplemental Digital Content 3, http://links.lww.com/ALN/C461, showing that registration preserved lung density distributions).

Analysis of Lung Inflation. In Step 4, we measured small-scale aeration changes by calculating the differences in x-ray film attenuation, measured in Hounsfield Units, between tissue voxels of warped-prone and supine images. Each voxel's Hounsfield Units value quantifies the increase or decrease of gas content in that same tissue unit. We quantified body position–related changes in the dimensions of each tissue voxel as its corresponding Jacobian.[19] A Jacobian is a unitless metric of tissue deformation calculated during image registration. When comparing corresponding warped-prone and supine images, a voxel with a negative determinant of the log Jacobian represents contraction, whereas a positive value indicates expansion incurred by the same lung tissue unit. Detailed analysis of lung recruitment was performed by identifying and mapping the voxels that shifted from the high density, nonaerated range (–100 to + 100 Hounsfield Units) to lower density ranges[20] when comparing the warped-prone to the supine images. Derecruitment was measured as voxels that increased density to higher than –101 Hounsfield Units when turning prone. Whole-lung contents of gas and tissue were estimated by density measurements on the nonregistered images.[21]

Cluster Analysis. K-means clustering was performed on the voxel distribution of Hounsfield Units (x-axis) and of Jacobian (y-axis) to characterize three different groups (reinflation, limited-change, and deflation). The number of clusters (k = 3) was chosen during preliminary analysis because it maintained physiologically plausible inflation responses and stable distributions among animals. Both Hounsfield Units and Jacobian were normalized by standard score [$(x - \mu)/\sigma$] to prevent bias due to the value dispersion between x- and y-axis (μ is the mean of the population and σ is the standard deviation of the population). For each cluster, the percentage of total lung mass and volume it occupied and its mean values of Hounsfield Units, Jacobian, and computed tomography intensity were calculated in each condition. Gravitational and nongravitational patterns of cluster distribution were separately investigated by partitioning the lung images into 10 horizontal and 10 vertical bins of equal mass.

Statistical Analysis

No power analysis was performed due to the retrospective design of the study. Descriptive statistics were performed on the clusters identified by K-means, characterizing their size as a percent fraction of total lung volume and mass, and their values of mean computed tomography intensity, Hounsfield Units, and Jacobian. All continuous data were reported as mean ± SD. Repeated-measures ANOVA was performed to compare the cluster distributions across spatial compartments. Two-tailed paired *t* tests were performed for relevant cluster distribution comparisons, and to compare physiologic values between data obtained at healthy baseline *versus* injury, prone *versus* supine, and lower *versus* higher PEEP. An experiment-wide $P < 0.05$ was selected as the threshold for statistical significance. Data was reformatted and prepared in Jupyter Notebook using Python 3.6. Statistical analysis was performed using RStudio 1.2.5001 (R Foundation for Statistical Computing, Austria).

Results

The imaging results are a reanalysis of a previously published computed tomography dataset from a pig model of mild lung injury. All animals survived and were included in the analysis. Hydrochloric acid injection caused mild lung injury, with a decrease in Pao_2 from 251.5 ± 50.4 to 161.1 ± 116.9 mmHg ($P = 0.047$), and with a decrease in respiratory system compliance from 20.1 ± 3.1 to 14.6 ± 4.2 ml/cm H_2O ($P = 0.046$) at PEEP 5 cm H_2O in the supine position (see table, Supplemental Digital Content 4, http://links.lww.com/ALN/C462, showing blood gases and respiratory mechanics data). After injury, the prone position

increased Pao_2 at both PEEP levels, but it did not affect compliance. Higher PEEP did not modify gas exchange or compliance.

Regional Lung Inflation

Representative baseline computed tomography images obtained before acid-induced lung injury are shown at inspiration with ventilation at PEEP 5 cm H_2O (fig. 2A) and at PEEP 10 cm H_2O (fig. 2B). The supine, prone, and corresponding warped-prone images are shown in the left panels of figure 2. The corresponding subtraction maps (fig. 2, middle panels) show negative Hounsfield Units values (blue) in the dorsal lung regions, indicating increased gas content from supine to prone. In contrast, density increased (positive Hounsfield Units values, in red) in the ventral lung, indicating locally reduced aeration when prone. The Jacobians extracted during registration of prone to supine images were mapped and displayed next to the subtraction maps (fig. 2, middle panels). Negative Jacobian values (blue) were visible in ventral lung regions, indicating tissue contraction in the prone position in the regions where Hounsfield Units were positive. In the dorsal regions, positive Jacobian values (red) dominated, indicating expansion in the regions where density decreased.

Postinjury images at PEEP 5 and 10 cm H_2O (fig. 3, A and B, left panels) show that, after registration, supine and warped-prone images differed only in the distribution of pulmonary densities, which were more prominent in the supine position. Similar to healthy baseline, the regional Hounsfield Units values at both PEEP levels were generally negative (improved aeration) in the dorsal lung and positive (decreased aeration) in the ventral regions (fig. 3, A and B, middle panels). The Jacobian maps also displayed similar behavior (ventral contraction, dorsal expansion) to that in healthy lungs.

Cumulative frequency distributions (including all animals) of Hounsfield Units and Jacobian values were more heterogeneous after injury (fig. 3, A and B, right panels) than in healthy conditions (fig. 2, A and B, right panels). Mean Hounsfield Units values were near zero in all the tested conditions, suggesting that the prone position had minimal net effect on whole-lung gas content. This was confirmed by the stability of mean lung density and whole-lung gas volumes between prone and supine positions (see table, Supplemental Digital Content 5, http://links.lww.com/ALN/C463, showing the results of computed tomography density analysis in the nonprocessed images).

Cluster Analysis

Cluster analysis assigned lung tissue voxels to clusters with distinct characteristics (fig. 4). The following cluster characterization represents general trends, derived from analysis of all conditions (table 1; see also figure, Supplemental Digital Content 6, http://links.lww.com/ALN/C464, with descriptive statistics of computed tomography–derived characteristics of each cluster). The most ventral cluster (blue, fig. 4) occupied on average (including all conditions studied) 39.0% of the total lung volume and 29.3% of total lung mass, and was characterized by positive Hounsfield Units and negative Jacobian values, indicating loss of aeration and tissue compression (deflation). The midlung cluster (black, fig. 4) occupied a larger fraction of lung tissue (47.0% of total lung volume and 47.6% of total mass, on average for all conditions), with small average values of Hounsfield Units and Jacobian suggesting limited response to position. The third cluster in the dorsal lung (red, fig. 4) had negative Hounsfield Units and positive Jacobian values, indicating reinflation, and was the smallest cluster (all-condition averages of 14.0% of total lung volume and 23.1% of total lung mass). Cluster percent distributions, Hounsfield Units, and Jacobian values were not significantly affected by injury *versus* healthy status. After injury, the reinflation cluster was smaller at PEEP 10 cm H_2O than at PEEP 5 cm H_2O ($P = 0.039$). Regional quantification of cluster distribution in 10 vertical and 10 horizontal bins of equal mass showed both ventro-dorsal and craniocaudal gradients (fig. 5). The 10 horizontal bins (fig. 5A) were partitioned evenly into dorsal and ventral compartments, while the vertical bins (fig. 5B) that interfaced the diaphragm were grouped into a caudal *versus* a cranial compartment. Cluster distribution significantly differed between both ventro-dorsal ($F[1, 4] = 103.9$, $P < 0.001$), and cranio-caudal compartments ($F[1, 4] = 117.5$, $P < 0.001$). Of the reinflation cluster, 86.4 ± 8.5% was located within the dorsal compartment *versus* 13.6 ± 8.5% in the ventral compartment ($P < 0.001$). Of the reinflation cluster, 63.4 ± 11.2% was contained in the caudal, peridiaphragmatic bins *versus* 36.6 ± 11.2% ($P < 0.001$) in the remaining bins.

Lung Recruitment

Figure 6 displays representative postinjury maps of recruitment and derecruitment due to prone position at end-inspiration at both PEEP 5 cm H_2O and PEEP 10 cm H_2O, with group mean ± SD values shown below each map. Prone positioning recruited 64.5 ± 36.7 g of tissue (11.4 ± 6.8% of total lung mass) at low PEEP and 49.9 ± 12.9 g (8.9 ± 2.8% of total mass) at higher PEEP. Of recruited voxels, 59.0 ± 13.0% were in the caudal region. Derecruitment was relatively small in both conditions. We also registered PEEP 5 and 10 cm H_2O images to each other for each position (left two columns) in order to visualize tissue with restored aeration at higher PEEP. The images show that this and position-related recruitment were quantitatively similar. Both recruitment and derecruitment were low in healthy lungs (see table, Supplemental Digital Content 7, http://links.lww.com/ALN/C465, showing recruitment and derecruitment data in all conditions).

Discussion

We directly visualized the effects of positioning on each unit of lung tissue in paired prone–supine computed

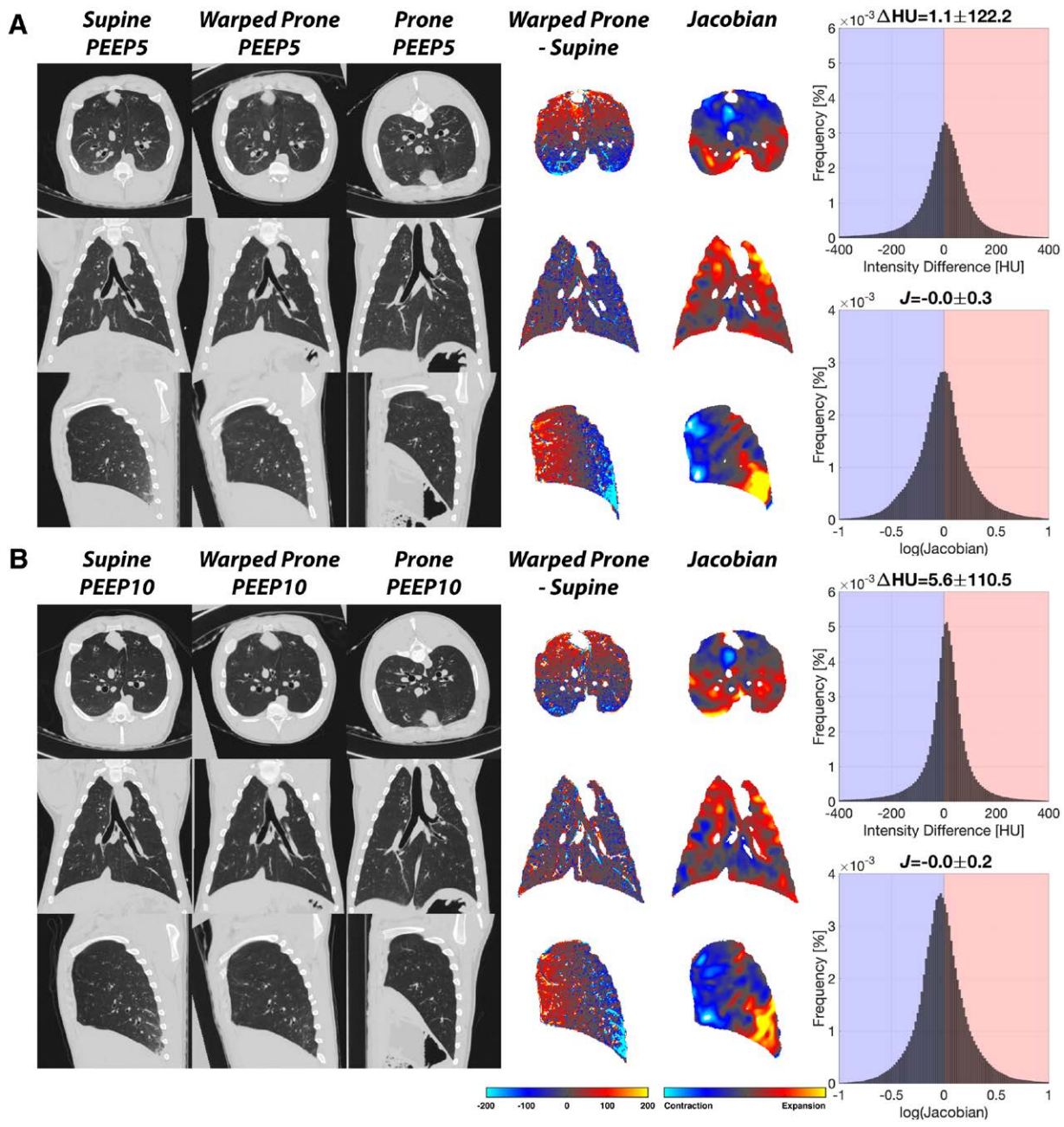

Fig. 2. Representative images obtained at baseline healthy conditions are shown in (*A*) at positive end-expiratory pressure (PEEP) 5 cm H_2O and in (*B*) at PEEP 10 cm H_2O. *Left panels*: Axial, coronal, and sagittal views of the target supine images, warped-prone image (shown inverted), and original (nonwarped) prone image. *Middle panel*: Subtraction maps plotting the density difference (ΔHU) between warped-prone and supine images are shown side by side with the Jacobian maps for each view. An expanding Jacobian value was associated with a decrease in density when changing position from supine to prone. *Right panels*: Cumulative frequency distributions of Hounsfield Unit (HU) and Jacobian values were plotted for the whole lung.

tomography scans of ventilated pigs. We then identified which regions of the lung responded to the prone position with reinflation, deflation, or limited change. These patterns followed both gravitational and nongravitational distributions: reinflation was mostly concentrated in the caudal lung region near the dorsal portion of the diaphragm (figs. 4 and 5). Recruitment of nonaerated tissue contributed to reinflation in this same region after injury (fig. 6).

Using image registration, we were able to match lung structures in paired images to provide a detailed

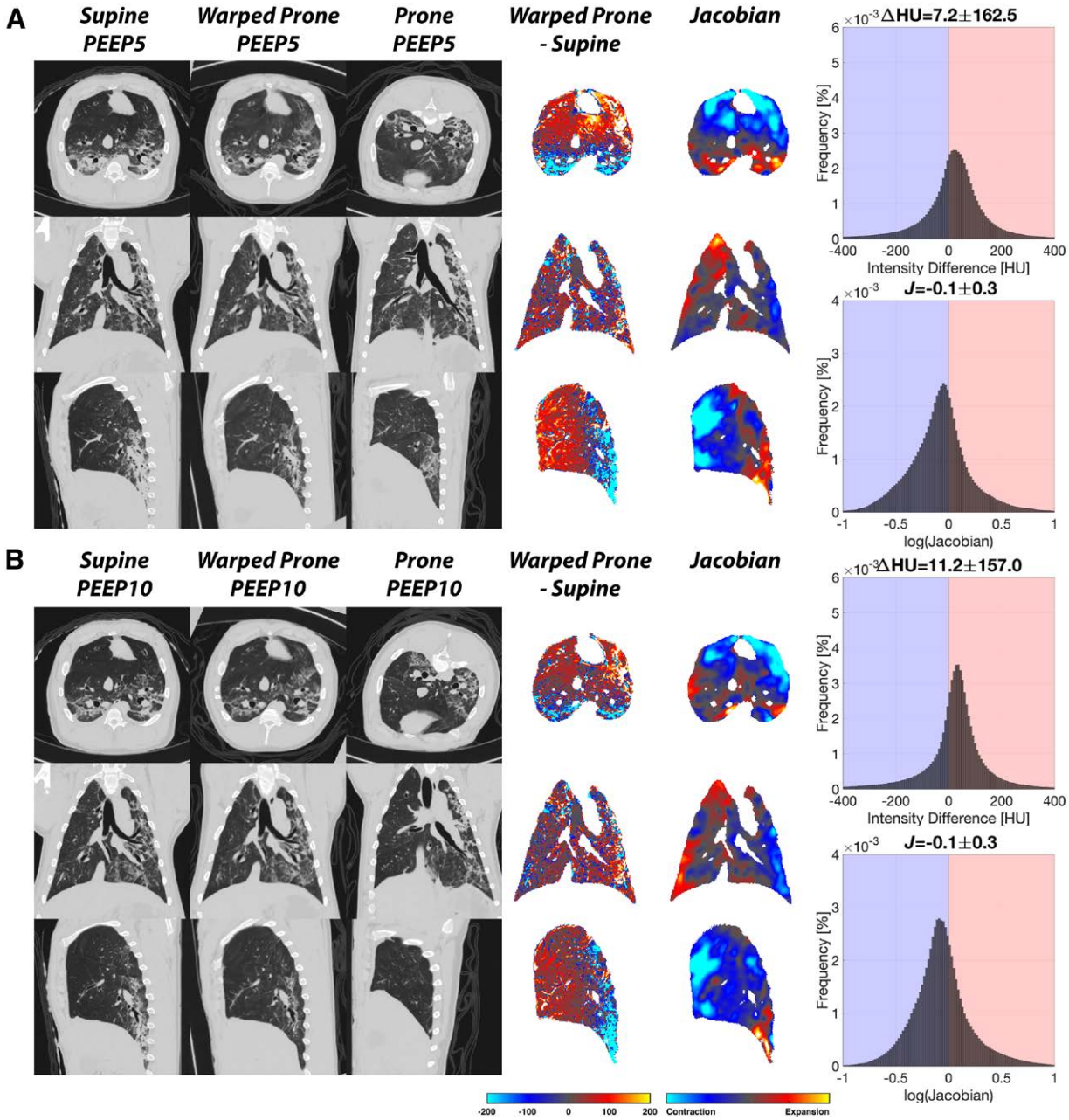

Fig. 3. Images were repeated in all tested conditions after lung injury induction by acid aspiration and are shown in (*A*) at positive end-expiratory pressure (PEEP) 5 cm H_2O and in (*B*) at PEEP 10 cm H_2O. The *left panels* show the target supine images, warped-prone image (shown inverted), and original (nonwarped) prone image. The *middle panel* shows the change of density in Hounsfield Units (ΔHU) and Jacobian maps side by side, with the corresponding cumulative frequency distribution in the *right panels*.

quantification of position-related changes in regional lung volume and gas content (figs. 2 and 3). After this step, cluster analysis grouped tissue units according to changes in density (aeration) and dimensions (expansion or contraction). We then mapped the spatial distribution of the three clusters, which had distinct responses to prone positioning: ventral deflation (increased density and contraction), limited tissue response in the midlung, and dorsal reinflation (decreased density and tissue expansion). We used K-means clustering,[22] with its simplicity and low computational complexity, to generate nonsubjective regions of interest that shared similar patterns of the two markers we presented in this work (density change and tissue deformation). This method is suitable for classifying an image into different regions when the

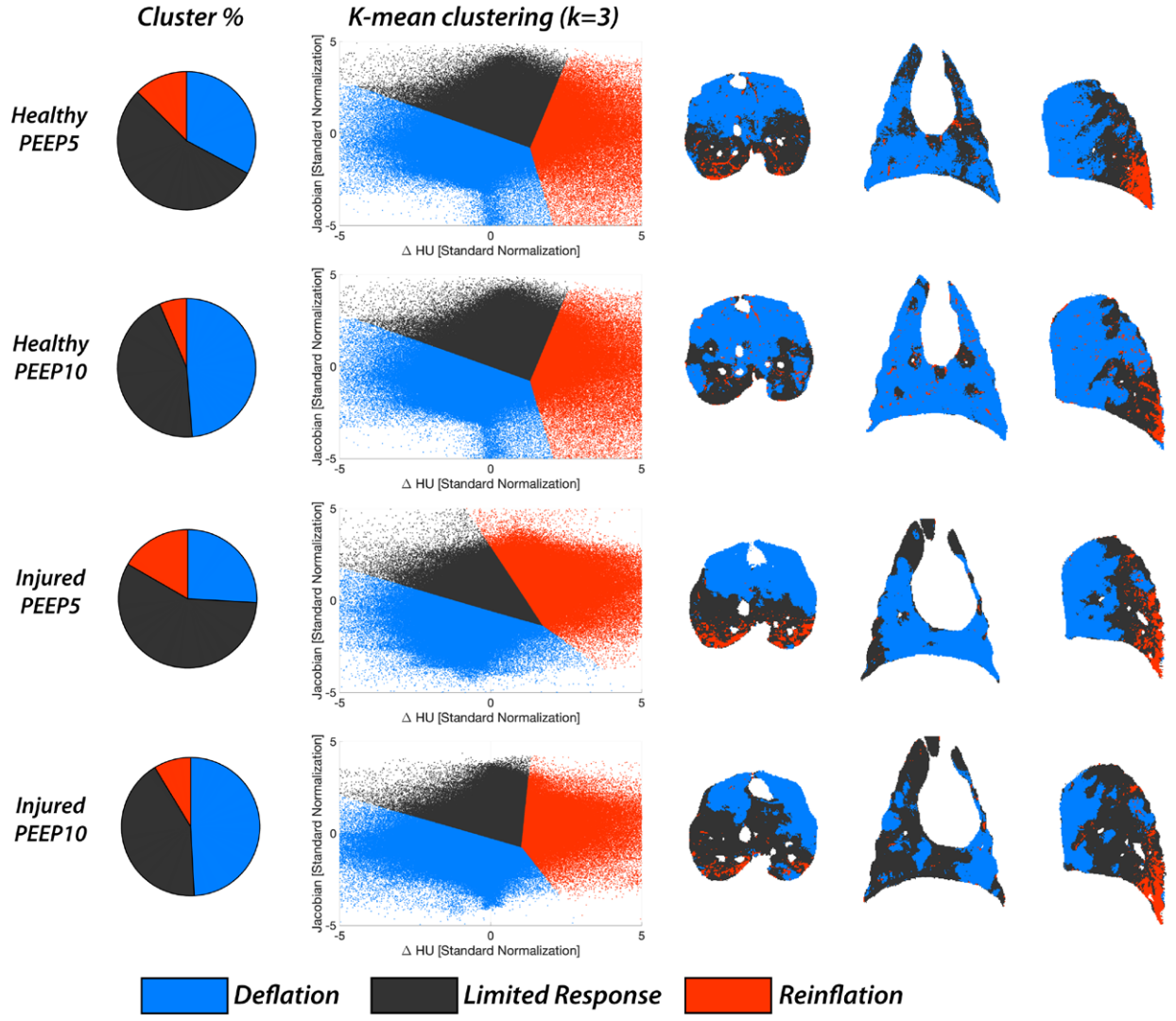

Fig. 4. Three-cluster K-mean analysis was performed on images obtained at healthy baseline and after injury at both positive end-expiratory pressure (PEEP) 5 and 10 cm H_2O at end-inspiration. On the *left*, frequency distributions of normalized change of density in Hounsfield Units (ΔHU) and Jacobian values are shown, with the identified three clusters highlighted in *blue* (deflation), *black* (limited response), and *red* (reinflation). On the *right*, the topographic distribution of voxels included in each cluster is shown in binary maps, using the same color scheme as in the frequency distributions. The maps show a distribution of the clusters along the vertical (gravitational) axis, although nongravitational heterogeneity was visible. In addition, the most dependent cluster was the smallest one and was located in the dorso-caudal regions of the lung.

number of clusters is known for particular human anatomy and/or physiology.[23,24] We postulated a three-cluster model, as it would reflect expected simple airspace responses. We are confident in this model, as it resulted in stable classifications between animals and conditions. Furthermore, the opposite density changes measured in the reinflation and deflation clusters were physiologically plausible.

Our methods allow us to quantify the effects of compressive phenomena on the distribution of aeration in the prone *versus* supine position. The observed ventral contraction and dorsal expansion of lung tissue corroborates studies proposing that attenuation of the gravitational gradient of lung density in prone ARDS patients[3] is due to redistribution of the forces that deform the lung,[7,25,26] causing more uniform pleural and transpulmonary pressures than in the supine position.[4,27] Additionally, we measured predominant reinflation and recruitment (after injury) in the dorso-caudal lungs, indicating localized positional responses near the diaphragm. The concurrent craniocaudal and ventro-dorsal aeration patterns confirm the coexistence of gravitational and nongravitational forces. This finding is in accordance with the results of a detailed *ex vivo* analysis of lung tissue, which showed that gravity does not dominate the topographic effects of position on lung function.[8] In

Table 1. Distributions of Lung Tissue among Clusters (Reinflation, Limited Response, Deflation) Are Shown for Each Tested Condition

		Healthy Baseline						Injury						*P* Value PEEP5 *vs.* PEEP10		*P* Value Healthy *vs.* Injury	
		PEEP5			PEEP10			PEEP5			PEEP10			Healthy	Injury	PEEP5	PEEP10
Cluster % by mass	Reinflation	17%	±	6%	15%	±	4%	27%	±	11%	18%	±	2%	0.170	**0.016**	0.603	0.458
	Limited response	54%	±	6%	45%	±	11%	39%	±	22%	44%	±	16%	0.827	0.746	0.388	0.715
	Deflation	30%	±	9%	40%	±	15%	34%	±	17%	38%	±	18%	0.179	0.132	0.572	0.833
Cluster % by volume	Reinflation	13%	±	7%	6%	±	2%	17%	±	12%	9%	±	2%	0.055	**0.039**	0.786	0.822
	Limited response	55%	±	7%	45%	±	11%	57%	±	10%	42%	±	19%	0.730	0.227	0.281	0.735
	Deflation	33%	±	10%	49%	±	13%	26%	±	12%	49%	±	21%	0.110	0.086	0.574	0.894

Cluster distribution was calculated (mean ±SD) as percent fraction of total mass and volume. Statistical comparisons are shown. Bold values indicate $P < 0.05$. PEEP, positive end-expiratory pressure.

fact, position-related changes to perfusion and ventilation were prominent in the dorso-caudal lung region of ventilated pigs,[8] which could be explained by focal compression and deflation in the same regions when animals are in the supine position. Such regional patterns result from the reconfiguration of the diaphragm profile that occurs with position due to changes in abdominal pressure.[4] These effects of positioning on the diaphragm are known,[28,29] but here we proved a first clear, direct visualization of their implications on regional lung inflation.

Our approach has additional advantages over the analysis used in previous imaging studies.[3] Registration of paired images yields detailed maps of density and tissue deformation, which are otherwise impossible to obtain. Because our

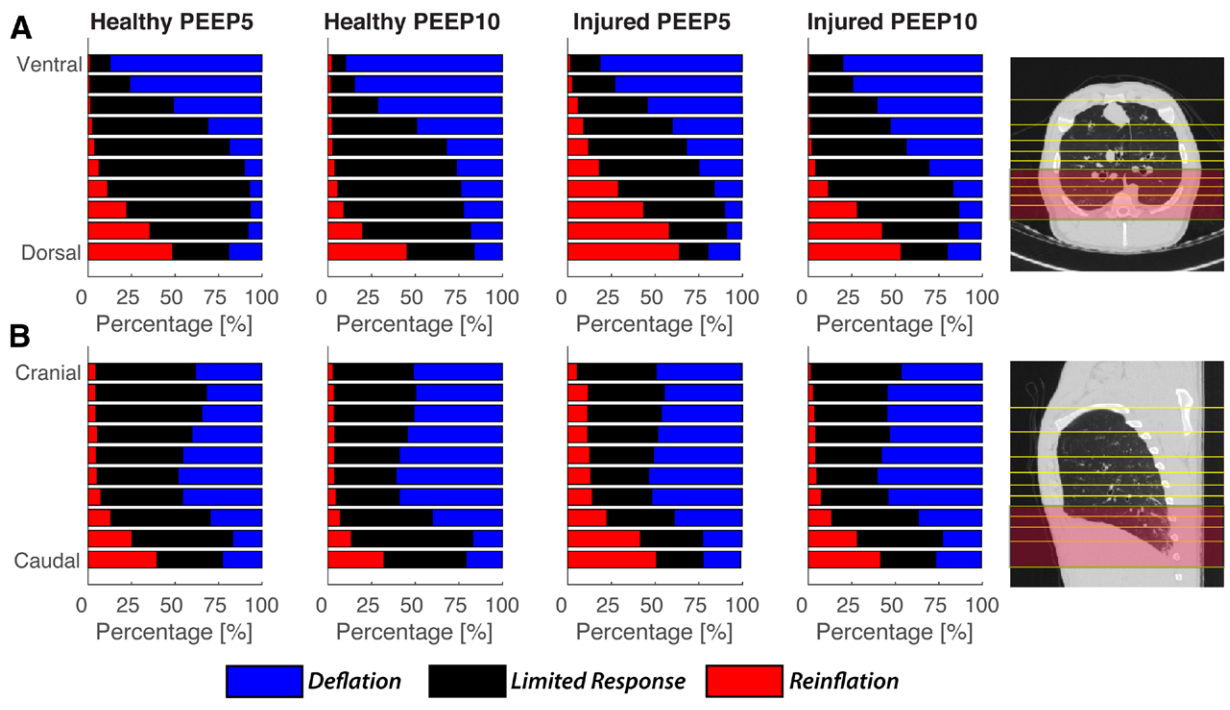

Fig. 5. Segment analysis among all end-expiratory conditions partitioned the lung into 10 segments of equal mass along the (*A*) dorsal-ventral axis and (*B*) the caudal-cephalad axis. The cluster frequencies of reinflation (*red*), limited response (*black*), and deflation (*blue*) are displayed at the level of each segment. The *far right* column shows the spatial orientation of the 10 equal mass segments that were used in the compartment analysis of cluster distribution. In (*A*), the *top five* segments correspond to the ventral compartment, and the *bottom five* segments are the dorsal compartment. In (*B*), segments that contain a pixel adjacent to the diaphragm are considered to be in the diaphragmatic compartment. The dorsal and caudal bins were shaded with *red color*. PEEP, positive end-expiratory pressure.

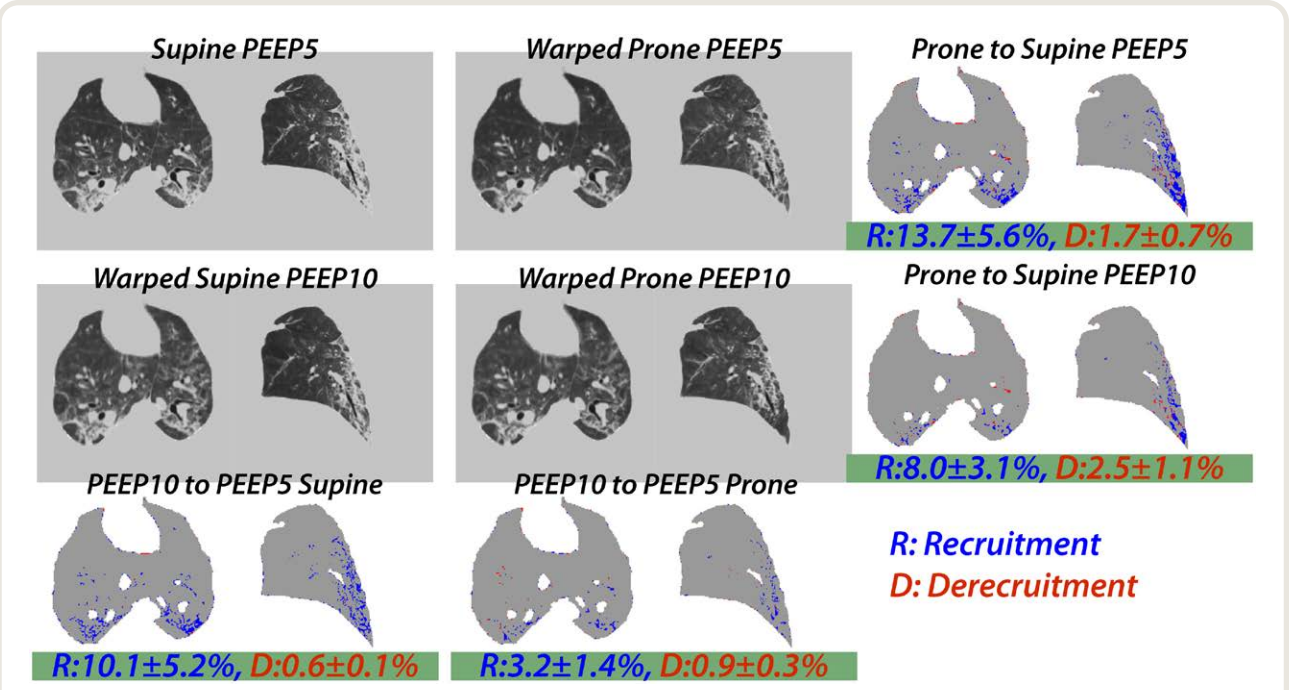

Fig. 6. Paired computed tomography scans obtained in the supine and prone positions are shown with the corresponding recruitment maps. Registration was performed between supine and prone images, yielding maps of position-related (from supine to prone) recruitment (R) and derecruitment (D) at positive end-expiratory pressure (PEEP) 5 cm H_2O (*top row*) and PEEP 10 cm H_2O (*second row*). Recruited voxels are shown in *blue*; derecruitment was small and shown in *red*. Numeric values are shown for each map. In addition, images at PEEP 5 and 10 cm H_2O were registered to each other, showing the PEEP-related recruitment in the supine and prone positions (*bottom row*).

voxel by voxel analysis does not impose constraints on the analysis (gravity or arbitrary density thresholds), the distribution of the clusters shows complexity that would be otherwise underappreciated. In fact, we detected voxels of different clusters intermingling with each other in the coronal maps (fig. 4), representing gravity-independent heterogeneity in response to position.

Prone position had negligible effects on the average density and gas volume of the whole lungs, results that are in discordance with studies where prone positioning improved lung capacity.[30] However, other studies reported stability of lung volumes when comparing prone to supine positions in animals[31] as well as in humans.[32] Similar to human studies,[33,34] we did not observe improvements in respiratory system compliance in the prone position. This absence of effect was likely related to compression of the ventral chest wall reducing chest wall compliance, which offset improvements in lung compliance.[35,36] We did not support shoulders and hips in the prone position, which restrains lung expansion and limits ventral inflation,[2,32] and likely caused density to increase in a large region of ventral lung (fig. 4).

In the setting of unchanged gas content, gas exchange improvements in the prone position were likely related to focally improved recruitment and ventilation-perfusion matching in the dorso-caudal region of the lung. Studies by others have quantified lung recruitment by prone position,[32,37] but registering paired images allowed us to map the reopening of collapsed tissue with voxel-level detail. As shown in figure 6, tissue voxels recruited by the prone position were dorsally distributed and were predominantly located within the dorso-caudal region occupied by the reinflation cluster. Dorsal recruitment was not matched by an equivalent amount of ventral derecruitment in this model. The net balance in favor of recruitment was compatible with the mild injury and dorsal distribution of the lesions, with less tendency for lung collapse in the ventral lung regions. Furthermore, density was more homogeneous between clusters in the prone compared to supine position (see panels C and D in Supplemental Digital Content 6, http://links.lww.com/ALN/C464, showing cluster densities in each position). Similar to previous studies,[38] such even aeration indicated reduced tendency for ventilation loss in the prone position. Oxygenation and recruitment improved in the prone position at both levels of PEEP; however, improvement in aeration due to higher PEEP (fig. 6) was not associated with improved oxygenation. This discrepancy was probably related to more favorable distributions of perfusion and of ventilation observed in the prone position *versus* higher PEEP.[39] However, a larger gradient between tested PEEP level could have revealed whether spatial patterns of reinflation are superimposable when comparing higher PEEP *versus* prone positioning.

Limitations

Our study has several limitations. First, the use of an animal model limits the extrapolation of our results to human ARDS. While the vertical distribution of computed tomography density in pigs is qualitatively similar to that reported in humans,[32] lung and thoracic geometries may be different. We studied a mild model of lung injury, but we showed significant radiologic changes and sizable oxygenation and recruitment responses to prone positioning. Furthermore, previous animal studies showed that prone positioning delays the progression of mild injury,[5,16] supporting the relevance of our results. The small number of animals also limits statistical power, but we were nevertheless able to effectively describe established gravitational and novel nongravitational effects of prone position on lung tissue. Registration is a key component of our analysis, and its use to study body position is novel. Validation of this methodology is ongoing within the field,[40] but we showed that peripheral pulmonary outlines, major airway structures, and density distributions were accurately superimposed when comparing warped-prone to supine images, indicating fidelity in the conservation of spatial coordinates between positions. We have displayed similar validations of these methods in our previous studies of tidal inflation in registered inspiratory–expiratory images.[41] Our study lacked esophageal manometry, and we cannot discriminate the effects of positioning on pulmonary and thoracic mechanics. Last, while we allowed 10 min of stabilization before imaging after each change in PEEP and body position, longer periods of stabilization may have elucidated greater changes in gas exchange and respiratory mechanics.

Implications

Our study is unique in that we were able to directly visualize improvements in small-scale aeration and match them with tissue expansion and local recruitment due to prone position. Although we did not directly test their biologic implications, these patterns are important because the effects of positional therapy on patient mortality are not explained by better gas exchange.[42] Therefore, imaging characteristics may be implicated in predicting injury progression and response to therapy. The current study shows that the beneficial effects of prone position on lung recruitment and aeration are concentrated in the same dorso-caudal region. It is therefore likely that the presence of opacifications in the dorsal lung and their responses to prone position (recruitment, reinflation) are key indicators of the therapeutic and protective effects of this therapy. Noninvasive imaging tools such as lung ultrasound[43] can assess localized responses in the dorso-caudal lung and possibly predict outcome and personalize care in individual patients.

Conclusions

We directly measured and mapped the effects of prone position on lung density and small-scale inflation, and found that improvements in both metrics were concentrated in the dorso-caudal region of the lung. These localized changes may help interpret positional therapy outcomes.

Acknowledgments

The authors thank the Center for Advanced Computed Tomography Imaging Services (CACTIS) at University of Pennsylvania (Philadelphia, Pennsylvania), especially Ms. Sheila Murdaugh (American Registry of Radiologic Technologists), who spent many weekends with us imaging the subjects.

Research Support

This work was supported by National Institues of Health (Bethesda, Maryland) grants R01-HL139066, R01-HL124986, and R01-HL137389.

Competing Interests

Dr. Cereda received grant support from Hillrom (Indiana). Dr. Gee received grant support from University of Electronic Science and Technology of China, International Neuroinformatics Coordinating Facility, Asian Society of Magnetic Resonance in Medicine, ShanghaiTech University, China. The remaining authors declare no competing interests.

Correspondence

Address correspondence to Dr. Cereda: Department of Anesthesiology and Critical Care, Perelman School of Medicine at the University of Pennsylvania, Dulles 773, 3400 Spruce Street, Philadelphia, Pennsylvania 19104-4283. maurizio.cereda@pennmedicine.upenn.edu.

References

1. Gattinoni L, Tognoni G, Pesenti A, Taccone P, Mascheroni D, Labarta V, Malacrida R, Di Giulio P, Fumagalli R, Pelosi P, Brazzi L, Latini R; Prone-Supine Study Group: Effect of prone positioning on the survival of patients with acute respiratory failure. N Engl J Med 2001; 345:568–73
2. Guérin C, Reignier J, Richard JC, Beuret P, Gacouin A, Boulain T, Mercier E, Badet M, Mercat A, Baudin O, Clavel M, Chatellier D, Jaber S, Rosselli S, Mancebo J, Sirodot M, Hilbert G, Bengler C, Richecoeur J, Gainnier M, Bayle F, Bourdin G, Leray V, Girard R, Baboi L, Ayzac L; PROSEVA Study Group: Prone positioning in severe acute respiratory distress syndrome. N Engl J Med 2013; 368:2159–68
3. Gattinoni L, Pelosi P, Vitale G, Pesenti A, D'Andrea L, Mascheroni D: Body position changes redistribute lung

computed-tomographic density in patients with acute respiratory failure. Anesthesiology 1991; 74:15–23
4. Mutoh T, Guest J, Lamm JE, Albert RK: Prone position alters the effect of volume overload on regional pleural pressures and improves hypoxemia in pigs in ViV01, 2. Am Rev Respir Dis 1992; 146:300–6
5. Motta-Ribeiro GC, Hashimoto S, Winkler T, Baron RM, Grogg K, Paula LFSC, Santos A, Zeng C, Hibbert K, Harris RS, Bajwa E, Vidal Melo MF: Deterioration of regional lung strain and inflammation during early lung injury. Am J Respir Crit Care Med 2018; 198:891–902
6. Perchiazzi G, Rylander C, Vena A, Derosa S, Polieri D, Fiore T, Giuliani R, Hedenstierna G: Lung regional stress and strain as a function of posture and ventilatory mode. J Appl Physiol (1985) 2011; 110:1374–83
7. Hubmayr RD, Walters BJ, Chevalier PA, Rodarte JR, Olson LE: Topographical distribution of regional lung volume in anesthetized dogs. J Appl Physiol Respir Environ Exerc Physiol 1983; 54:1048–56
8. Altemeier WA, McKinney S, Krueger M, Glenny RW: Effect of posture on regional gas exchange in pigs. J Appl Physiol (1985) 2004; 97:2104–11
9. Gattinoni L, Taccone P, Carlesso E, Marini JJ: Prone position in acute respiratory distress syndrome. Rationale, indications, and limits. Am J Respir Crit Care Med 2013; 188:1286–93
10. Altemeier WA, McKinney S, Glenny RW: Fractal nature of regional ventilation distribution. J Appl Physiol (1985) 2000; 88:1551–7
11. Avants BB, Epstein CL, Grossman M, Gee JC: Symmetric diffeomorphic image registration with cross-correlation: Evaluating automated labeling of elderly and neurodegenerative brain. Med Image Anal 2008; 12:26–41
12. Avants BB, Tustison NJ, Stauffer M, Song G, Wu B, Gee JC: The Insight ToolKit image registration framework. Front Neuroinform 2014; 8:44
13. Galbán CJ, Han MK, Boes JL, Chughtai KA, Meyer CR, Johnson TD, Galbán S, Rehemtulla A, Kazerooni EA, Martinez FJ, Ross BD: Computed tomography-based biomarker provides unique signature for diagnosis of COPD phenotypes and disease progression. Nat Med 2012; 18:1711–5
14. Kaczka DW, Cao K, Christensen GE, Bates JH, Simon BA: Analysis of regional mechanics in canine lung injury using forced oscillations and 3D image registration. Ann Biomed Eng 2011; 39:1112–24
15. Reinhardt JM, Ding K, Cao K, Christensen GE, Hoffman EA, Bodas SV: Registration-based estimates of local lung tissue expansion compared to xenon CT measures of specific ventilation. Med Image Anal 2008; 12:752–63
16. Xin Y, Cereda M, Hamedani H, Pourfathi M, Siddiqui S, Meeder N, Kadlecek S, Duncan I, Profka H, Rajaei J, Tustison NJ, Gee JC, Kavanagh BP, Rizi RR: Unstable inflation causing injury. Insight from prone position and paired computed tomography scans. Am J Respir Crit Care Med 2018; 198:197–207
17. Tustison NJ, Avants BB: Explicit B-spline regularization in diffeomorphic image registration. Front Neuroinform 2013; 7:39
18. Xin Y, Song G, Cereda M, Kadlecek S, Hamedani H, Jiang Y, Rajaei J, Clapp J, Profka H, Meeder N, Wu J, Tustison NJ, Gee JC, Rizi RR: Semiautomatic segmentation of longitudinal computed tomography images in a rat model of lung injury by surfactant depletion. J Appl Physiol (1985) 2015; 118:377–85
19. Christensen GE, Johnson HJ: Consistent image registration. IEEE Trans Med Imaging 2001; 20:568–82
20. Gattinoni L, Pesenti A, Avalli L, Rossi F, Bombino M: Pressure-volume curve of total respiratory system in acute respiratory failure. Computed tomographic scan study. Am Rev Respir Dis 1987; 136:730–6
21. Wandtke JC, Hyde RW, Fahey PJ, Utell MJ, Plewes DB, Goske MJ, Fischer HW: Measurement of lung gas volume and regional density by computed tomography in dogs. Invest Radiol 1986; 21:108–17
22. Ahmad A, Dey L: A k-mean clustering algorithm for mixed numeric and categorical data. Data Knowledge Eng 2007; 63:503–27
23. Selvakumar J, Lakshmi A, Arivoli T: Brain tumor segmentation and its area calculation in brain MR images using K-mean clustering and Fuzzy C-mean algorithm. Nagapattinam, Tamil Nadu, India, IEEE-International Conference On Advances In Engineering, Science And Management (ICAESM-2012). 2012, pp 186–90
24. Ng P, Pun C-M: Skin color segmentation by texture feature extraction and K-mean clustering, 2011 Third International Conference on Computational Intelligence, Communication Systems and Networks. Bali, Indonesia, IEEE, 2011, pp 213–8 doi:10.1109/CICSyN.2011.54
25. Liu S, Margulies SS, Wilson TA: Deformation of the dog lung in the chest wall. J Appl Physiol (1985) 1990; 68:1979–87
26. Hoffman EA: Effect of body orientation on regional lung expansion: a computed tomographic approach. J Appl Physiol (1985) 1985; 59:468–80
27. Lai-Fook SJ, Rodarte JR: Pleural pressure distribution and its relationship to lung volume and interstitial pressure. J Appl Physiol (1985) 1991; 70:967–78
28. Krayer S, Rehder K, Vettermann J, Didier EP, Ritman EL: Position and motion of the human diaphragm during anesthesia-paralysis. Anesthesiology 1989; 70:891–8
29. Mure M, Glenny RW, Domino KB, Hlastala MP: Pulmonary gas exchange improves in the prone position with abdominal distension. Am J Respir Crit Care Med 1998; 157(6 Pt 1):1785–90
30. Santini A, Protti A, Langer T, Comini B, Monti M, Sparacino CC, Dondossola D, Gattinoni L: Prone

position ameliorates lung elastance and increases functional residual capacity independently from lung recruitment. Intensive Care Med Exp 2015; 3:55
31. Albert RK, Leasa D, Sanderson M, Robertson HT, Hlastala MP: The prone position improves arterial oxygenation and reduces shunt in oleic-acid-induced acute lung injury. Am Rev Respir Dis 1987; 135:628–33
32. Cornejo RA, Díaz JC, Tobar EA, Bruhn AR, Ramos CA, González RA, Repetto CA, Romero CM, Gálvez LR, Llanos O, Arellano DH, Neira WR, Díaz GA, Zamorano AJ, Pereira GL: Effects of prone positioning on lung protection in patients with acute respiratory distress syndrome. Am J Respir Crit Care Med 2013; 188:440–8
33. Pelosi P, Tubiolo D, Mascheroni D, Vicardi P, Crotti S, Valenza F, Gattinoni L: Effects of the prone position on respiratory mechanics and gas exchange during acute lung injury. Am J Respir Crit Care Med 1998; 157:387–93
34. Mancebo J, Fernández R, Blanch L, Rialp G, Gordo F, Ferrer M, Rodríguez F, Garro P, Ricart P, Vallverdú I, Gich I, Castaño J, Saura P, Domínguez G, Bonet A, Albert RK: A multicenter trial of prolonged prone ventilation in severe acute respiratory distress syndrome. Am J Respir Crit Care Med 2006; 173:1233–9
35. Pelosi P, Bottino N, Chiumello D, Caironi P, Panigada M, Gamberoni C, Colombo G, Bigatello LM, Gattinoni L: Sigh in supine and prone position during acute respiratory distress syndrome. Am J Respir Crit Care Med 2003; 167:521–7
36. Kumaresan A, Gerber R, Mueller A, Loring SH, Talmor D: Effects of prone positioning on transpulmonary pressures and end-expiratory volumes in patients without lung disease. Anesthesiology 2018; 128:1187–92
37. Galiatsou E, Kostanti E, Svarna E, Kitsakos A, Koulouras V, Efremidis SC, Nakos G: Prone position augments recruitment and prevents alveolar overinflation in acute lung injury. Am J Respir Crit Care Med 2006; 174:187–97
38. Richter T, Bellani G, Scott Harris R, Vidal Melo MF, Winkler T, Venegas JG, Musch G: Effect of prone position on regional shunt, aeration, and perfusion in experimental acute lung injury. Am J Respir Crit Care Med 2005; 172:480–7
39. Richard JC, Bregeon F, Costes N, Bars DL, Tourvieille C, Lavenne F, Janier M, Bourdin G, Gimenez G, Guerin C: Effects of prone position and positive end-expiratory pressure on lung perfusion and ventilation. Crit Care Med 2008; 36:2373–80
40. Murphy K, van Ginneken B, Reinhardt JM, Kabus S, Ding K, Deng X, Cao K, Du K, Christensen GE, Garcia V, Vercauteren T, Ayache N, Commowick O, Malandain G, Glocker B, Paragios N, Navab N, Gorbunova V, Sporring J, de Bruijne M, Han X, Heinrich MP, Schnabel JA, Jenkinson M, Lorenz C, Modat M, McClelland JR, Ourselin S, Muenzing SE, Viergever MA, De Nigris D, Collins DL, Arbel T, Peroni M, Li R, Sharp GC, Schmidt-Richberg A, Ehrhardt J, Werner R, Smeets D, Loeckx D, Song G, Tustison N, Avants B, Gee JC, Staring M, Klein S, Stoel BC, Urschler M, Werlberger M, Vandemeulebroucke J, Rit S, Sarrut D, Pluim JP: Evaluation of registration methods on thoracic CT: the EMPIRE10 challenge. IEEE Trans Med Imaging 2011; 30:1901–20
41. Cereda M, Xin Y, Hamedani H, Bellani G, Kadlecek S, Clapp J, Guerra L, Meeder N, Rajaei J, Tustison NJ, Gee JC, Kavanagh BP, Rizi RR: Tidal changes on CT and progression of ARDS. Thorax 2017; thoraxjnl-2016-209833 doi:10.1136/thoraxjnl-2016-209833
42. Albert RK, Keniston A, Baboi L, Ayzac L, Guérin C; Proseva Investigators: Prone position-induced improvement in gas exchange does not predict improved survival in the acute respiratory distress syndrome. Am J Respir Crit Care Med 2014; 189:494–6
43. Goffi A, Kruisselbrink R, Volpicelli G: The sound of air: Point-of-care lung ultrasound in perioperative medicine. Can J Anaesth 2018; 65:399–416